

PICAR: An Efficient Extendable Approach for Fitting Hierarchical Spatial Models

Benjamin Seiyon Lee and
Murali Haran*
Department of Statistics,
Pennsylvania State University

May 17, 2022

Abstract

Hierarchical spatial models are very flexible and popular for a vast array of applications in areas such as ecology, social science, public health, and atmospheric science. It is common to carry out Bayesian inference for these models via Markov chain Monte Carlo (MCMC). Each iteration of the MCMC algorithm is computationally expensive due to costly matrix operations. In addition, the MCMC algorithm needs to be run for more iterations because the strong cross-correlations among the spatial latent variables result in slow mixing Markov chains. To address these computational challenges, we propose a projection-based intrinsic conditional autoregression (PICAR) approach, which is a discretized and dimension-reduced representation of the underlying spatial random field using empirical basis functions on a triangular mesh. Our approach exhibits fast mixing as well as a considerable reduction in computational cost per iteration. PICAR is computationally efficient and scales well to high dimensions. It is also automated and easy to implement for a wide array of user-specified hierarchical spatial models. We show, via simulation studies, that our approach performs well in terms of parameter inference and prediction. We provide several examples to illustrate the applicability of our method, including (i) a parasitic tree infestation data set that showcases its computational efficiency in high-dimensional applications, (ii) a spatially varying coefficient model that demonstrates the ease of implementation of PICAR in the probabilistic programming language `stan`, and (iii) a watershed survey example that illustrates how PICAR applies to models that are not amenable to efficient inference via existing methods.

Keywords: basis representation, Markov chain Monte Carlo, Gaussian random field, non-Gaussian spatial data, spatially varying coefficients, ordinal spatial data

*Corresponding Author: mharan@stat.psu.edu

1 Introduction

Hierarchical spatial models are commonly used to model spatial observations across many fields, for example species abundance in ecology, ice presence in glaciology, geo-referenced survey responses in public health studies, and crime incidence in urban areas. A quick search suggests that hierarchical spatial models are featured in thousands of research papers published annually. An important class of hierarchical spatial models is the spatial generalized linear mixed model (SGLMM). These are flexible models for both point referenced and areal data, where Gaussian random fields are used to model the spatial dependence across locations (Diggle et al., 1998). Other examples of hierarchical spatial models include spatially varying coefficient processes (Gelfand et al., 2003; Mu et al., 2018), covariate measurement error models (Xia and Carlin, 1998; Bernadinelli et al., 1997; Muff et al., 2015), and co-regionalization models for multivariate responses (Banerjee et al., 2014). Hierarchical spatial models pose considerable computational challenges due to the large number of highly correlated spatial random effects which result in both costly likelihood evaluations and slow mixing in Markov Chain Monte Carlo (MCMC) algorithms.

In this manuscript, we provide a computationally efficient approach for fitting high-dimensional hierarchical spatial models by decorrelating and reducing the dimensions of the spatial random effects. What sets our projection-based intrinsic conditional autoregression (PICAR) approach apart from existing methods is: (i) our approach to dimension reduction and decorrelation of the random effects is efficient and automated; (ii) our approach is easily extendable, that is, it can be easily integrated into a hierarchical modeling scenario using implementations like the probabilistic programming language `stan` (Carpenter et al., 2017);

and (iii) our method scales well to higher dimensional hierarchical spatial models than is typical of existing methods. A major advantage of PICAR is that in addition to providing an efficient estimation approach for large datasets, it is easy for non-experts to specify general hierarchical spatial models of their choice in this framework.

Many innovative computational methods have been developed for high-dimensional spatial data in recent years (cf. Cressie and Johannesson, 2008; Banerjee et al., 2008; Higdon, 1998; Nychka et al., 2015; Lindgren et al., 2011; Katzfuss, 2017; Datta et al., 2016; Banerjee et al., 2013). Recent studies (Heaton et al., 2019; Bradley et al., 2016; Sun et al., 2012) examine several of these methods within the context of modeling high-dimensional spatial data. However, these methods primarily focus on linear spatial models with Gaussian observations. Notable exceptions are predictive process (Banerjee et al., 2008) and random projections (Guan and Haran, 2018), which use a low-dimensional representations of the latent random field. However, these require updating the basis functions at each iteration of the MCMC algorithm. Bradley et al. (2019) provides a employ a basis representation of the latent random field while also exploiting conjugate distributions. However, the full conditional distributions may be difficult to construct as they require computing many matrices, vectors, and constants, and there are also open questions regarding the mixing of the resulting Gibbs samplers. INLA (Rue et al., 2009; Lindgren et al., 2011) provides a very fast approximation of the posterior distribution. While this approach is applicable to a wide array of models, it is not always easily extendable to user-specified hierarchical spatial models. We provide more discussion about these algorithms later in the manuscript.

Our method addresses computational challenges by representing the spatial random

effects with empirical basis functions. Various basis representations have been directly or indirectly used to model spatial data, for instance in the predictive process approach (Banerjee et al., 2008), random projections (Guan and Haran, 2018, 2019; Banerjee et al., 2013; Park and Haran, 2019), Moran’s basis for areal models (Hughes and Haran, 2013), stochastic partial differential equations (Lindgren et al., 2011), kernel convolutions (Higdon, 1998), eigenvector spatial filtering (Griffith, 2003), and multi-resolution basis functions (Nychka et al., 2015; Katzfuss, 2017), among others. We utilize a set of basis functions inspired by the Moran’s I statistic and piece-wise linear basis functions. To our knowledge, this is the first approach that readily lends itself to user-specified hierarchical spatial models while also remaining computationally efficient for large datasets. We demonstrate the applicability of PICAR via simulation studies as well as high-dimensional datasets from a forest resource management study and a watershed water quality survey.

The rest of the paper is organized as follows. In Section 2, we describe hierarchical spatial models and discuss their computational challenges. In Section 3, we describe our PICAR approach in detail. In Section 4, we present simulated examples for: (i) a spatial model for binary observations; (ii) a spatially varying coefficient model for count observations, implemented in PICAR using `stan`; and (iii) a model for ordered categorical spatial data that cannot be fit using existing publicly available code but can be easily fit using PICAR. In Section 5 we apply PICAR to two large spatial datasets: occurrence of a parasitic species of dwarf mistletoe in Minnesota and water quality ratings in Maryland watersheds. Finally, we provide a summary and directions for future research in Section 6.

2 Hierarchical Spatial Models

We begin by describing a general framework for hierarchical spatial models and provide several examples that will be explored in depth via simulation studies. We also provide a general discussion of the computational challenges for fitting these models.

2.1 Model Specification

Let $Z(s)$ denote a spatial process at location s in a spatial domain $\mathcal{D} \subset \mathbb{R}^d$ where d is typically 2 or 3. We define $Z(s)$ as:

$$Z(s) = X(s)\beta + w(s) + \epsilon(s), \text{ for } s \in D, \tag{1}$$

where $X(s)$ is a set of k covariates associated with location s and β is a k -dimensional vector of coefficients. The micro-scale measurement errors or nugget are modeled as an uncorrelated Gaussian process with zero mean and variance τ^2 where $\epsilon(s) \sim N(0, \tau^2)$.

We impose spatial dependence by modeling the spatial random effects $\mathbf{W} = \{w(s) : s \in \mathcal{D}\}$ as a stationary zero-mean Gaussian process with a positive definite covariance function $C(\cdot)$. For a finite set of locations $s = (s_1, \dots, s_n)$, the spatial random effects \mathbf{W} are distributed as a multivariate normal distribution $\mathbf{W}|\Theta \sim N(0, C(\Theta))$ with covariance function parameters Θ and the covariance matrix $C(\Theta)$ where $C(\Theta)_{ij} = \text{cov}(w(s_i), w(s_j))$. The Matérn covariance function is a widely used class of stationary and isotropic covariance

functions (Stein, 2012) with parameters $\Theta = (\sigma^2, \phi, \nu)$ such that:

$$C(s_i, s_j) = \sigma^2 \frac{1}{\Gamma(\nu)2^{\nu-1}} \left(\sqrt{(2\nu)\frac{h}{\phi}} \right)^\nu K_\nu \left(\sqrt{(2\nu)\frac{h}{\phi}} \right),$$

where $R(\phi)$ is the correlation matrix, $h = \|s_i - s_j\|$ is the Euclidean distance between locations s_i and s_j , $\sigma^2 > 0$ is the partial sill or scale parameter of the process, and $\phi > 0$ is the range parameter for spatial dependence. $K_\nu(\cdot)$ is the modified Bessel function of the second kind where the smoothness parameter ν is commonly fixed prior to model fitting.

Hierarchical spatial models may be broadly described as (cf. Wikle et al., 1998):

Data Model: Observations $Z(s)|\mathbf{W}$, data model parameters

Process Model: $\mathbf{W}|$ covariance function parameters

Parameter Model: priors for parameters

In Sections 4 and 5 we discuss the implementation of PICAR in the context of several examples of hierarchical spatial models, including spatial generalized linear mixed models for non-Gaussian data, a spatially varying coefficient model, and a cumulative-logit model for ordered categorical data. These models roughly follow the same hierarchical structure as above, for example spatial generalized mixed models have the same process and parameter models with the data model replaced with a generalized linear model framework.

2.2 Model Fitting and Computational Challenges

The computational challenges are rooted in the dimensionality and correlation of the spatial random effects \mathbf{W} . Hierarchical spatial models typically require a costly evaluation of an n -dimensional multivariate normal likelihood function ($\mathcal{O}(n^3)$) at each iteration of the MCMC algorithm. Moreover, highly correlated spatial random effects can lead to poor mixing in MCMC algorithms (cf. Christensen et al., 2006; Haran et al., 2003).

There is a large literature on addressing computational challenges in spatial models though the vast majority of methods are focused on linear Gaussian spatial models. Popular approaches include low-rank approximations (Cressie and Johannesson, 2008; Banerjee et al., 2008), compact support or covariance tapering (Furrer et al., 2006; Stein, 2013), multiresolution approaches (Nychka et al., 2015; Katzfuss, 2017), and sparse representations of the $n \times n$ precision matrix via spatial partial differential equations (Lindgren et al., 2011) or nearest-neighbor processes (Datta et al., 2016). These typically focus on the marginal distribution of the spatial observations $\mathbf{Z} = (Z(s_1), \dots, Z(s_n))$, where $\mathbf{Z}|\beta, \sigma^2, \phi, \tau^2 \sim \mathcal{N}(X\beta, \Sigma(\sigma^2, \phi, \tau^2))$, and do not involve the high-dimensional latent spatial variables. Hence, they are not easily extended to more complex hierarchical spatial models.

For hierarchical spatial models with non-Gaussian observations (e.g. SGLMMs), Sengupta and Cressie (2013) and Sengupta et al. (2016) extend fixed-rank kriging (Cressie and Johannesson, 2008) to non-gaussian satellite imagery by: (1) representing the spatial random effects using bi-square basis functions; (2) estimating the model parameters via the expectation-maximization (EM) algorithm; and (3) embedding Laplace approximations in the E-step to improve computational efficiency. The predictive process approach

(Banerjee et al., 2008) also implements a basis representation of the spatial random effects $W(s) \in \mathbb{R}^n$. Prior to model fitting, m reference locations or knots $s^* = \{s_1^*, s_1^*, \dots, s_m^*\}$ are selected where $m \ll n$. Predictive processes approximates the spatial random effects such that $W(s) \approx C(s, s^*)C^{*-1}W(s^*)$, where $W(s^*)$ are the realizations of the Gaussian random field at knot locations s^* , $C^* = C(s^*, s^*)$ represents the $m \times m$ covariance matrix corresponding to the knots, and $C(s, s^*)$ denotes the cross-covariance between the observed locations (s) and the knot locations (s^*). Knots can be selected using an adaptive approach based on point-processes (Guhaniyogi et al., 2011). Note that the computational speedup comes from utilizing a lower-dimensional set of spatial random effects $W(s^*)$ and an $m \times m$ covariance matrix. However, predictive process must construct the basis functions matrix $C(s, s^*)C^{*-1}$ at each iteration of the algorithm, which incurs a cost of roughly $O(m^3 + nm^2)$. In PICAR, the basis constructions is only done once, and the costs for each iteration are linear in p , where p is the dimension of the dimension-reduced spatial random effects.

Guan and Haran (2018) use random projections to generate approximate eigenvector basis functions. The basis functions are linked to the Matérn class of covariance functions. The dominant computational cost is driven by large matrix-to-matrix multiplications, which can be easily parallelized. The spatial random effects are approximated as $W(s) \approx \tilde{U}_m \tilde{D}_m^{1/2} \delta$, where \tilde{U}_m and \tilde{D}_m are the first m approximate eigencomponents of the covariance matrix $\sigma^2 R_\phi$ for SGLMMs and δ are the m -dimensional reparameterized spatial random effects. While this approach bypasses knot selection, it still requires repeated constructions of the approximate eigenvector basis functions with a cost of $O(m^3 + nm^2)$.

Re-parameterization approaches (Christensen et al., 2006; Haran et al., 2003; Guan and

Haran, 2018) decorrelate the spatial random effects, which often results in faster mixing MCMC algorithms. However, these techniques can be very expensive for high-dimensional data since the reparameterization step is expensive and the number of random effects is unchanged. Data augmentation approaches (De Oliveira, 2000; Albert and Chib, 1993) apply to some classes of hierarchical models, resulting in a Gibbs sampler for the spatial random effects, but this still requires large matrix operations on dense covariance matrices, and does not necessarily address mixing issues in the resulting MCMC algorithm.

3 PICAR Approach

In this section, we present our projection-based intrinsic conditional autoregression (PICAR) approach that is designed to efficiently fit hierarchical spatial models. In this framework, we represent spatial random effects $\mathbf{W} = (W(s_1), W(s_2), \dots, W(s_n))$ as a linear combination of basis functions:

$$\mathbf{W} \approx \mathbf{\Phi}\delta \quad , \quad \delta \sim \mathcal{N}(0, \Sigma_\delta),$$

where $\mathbf{\Phi}$ is an $n \times p$ basis function matrix where each column denotes a basis function, $\delta \in \mathbb{R}^p$ are the re-parameterized spatial random effects (or basis coefficients), and Σ_δ is the $p \times p$ covariance matrix for the weights. Basis functions can be interpreted as a set of distinct spatial patterns that can be used to construct a spatial random field, along with their coefficients. Basis representation has been a popular approach to model spatial data (cf. Cressie and Johannesson, 2008; Banerjee et al., 2008; Hughes and Haran, 2013; Lindgren et al., 2011; Rue et al., 2009; Christensen et al., 2006; Haran et al., 2003;

Griffith, 2003; Higdon, 1998; Nychka et al., 2015). Examples of basis functions include splines, wavelets, empirical orthogonal functions, combinations of sines and cosines, piece-wise linear functions, and many others. Basis representations tend to be computationally efficient as they help bypass large matrix operations, reduce the dimensions of the spatial random effects, and as in our case, decorrelate the spatial random effects \mathbf{W} .

3.1 Projection-based Intrinsic Conditional Auto-Regression (PICAR)

The PICAR approach can be outlined as follows:

1. Generate a triangular mesh on the spatial domain $\mathcal{D} \subset \mathbb{R}^2$.
2. Construct a spatial field on the mesh nodes using data-driven basis functions.
3. Interpolate onto the observation locations using piece-wise linear basis functions.

We provide details for each step below.

Mesh Construction

Prior to fitting the model, we generate a mesh enveloping the observed spatial locations via Delaunay Triangulation (Hjelle and Dæhlen, 2006). Here, we divide the spatial domain D into a collection of non-intersecting irregular triangles. The triangles can share a common edge, corner (i.e. nodes or vertices), or both. The mesh generates a latent undirected graph $G = \{V, E\}$, where $V = \{1, 2, \dots, m\}$ are the mesh vertices and E are the edges. Each edge E is represented as a pair (i, j) denoting the connection between i and j . The graph G is characterized by its weights matrix \mathbf{W} , an $m \times m$ matrix where $A_{ii} = 0$ and $A_{ij} = 1$

when mesh node i is connected to node j and $A_{ij} = 0$ otherwise. The triangular mesh is built using the **R-INLA** package (Lindgren et al., 2015). Guidelines for mesh construction are provided in Lindgren et al. (2015), and details pertaining to algorithms for Delaunay triangulation can be found in Hjelle and Dæhlen (2006).

Moran’s Basis Functions

We generate a spatial random field on the set of mesh vertices V of graph G using the Moran’s basis functions (Hughes and Haran, 2013; Griffith, 2003). Griffith (2003) propose an augmented hierarchical spatial model (spatial eigenfiltering) using a subset of eigenvectors of the Moran’s operator $(\mathbf{I} - \mathbf{1}\mathbf{1}'/m)\mathbf{W}(\mathbf{I} - \mathbf{1}\mathbf{1}'/m)$, where \mathbf{I} is the identity matrix and $\mathbf{1}$ is a vector of 1’s. The operator appears in the numerator of the Moran’s I statistic, which is a diagnostic of spatial dependence (Moran, 1950) typically used for areal spatial data. Positive eigencomponents of the Moran’s operator correspond to varying magnitudes and patterns of positive spatial dependence. For the triangular mesh, the positive eigenvectors represent the patterns of spatial dependence among the mesh nodes, and their corresponding eigenvalues denote the magnitude of spatial dependence. Figure 1 illustrates the first 25 eigenvectors of the Moran’s operator.

We construct the Moran’s basis function matrix $\mathbf{M} \in \mathbb{R}^{m \times p}$, by selecting the first p eigenvectors of the Moran’s operator where $p \ll m$. In Section 3.3, we provide an automated heuristic for selecting a suitable rank p . We can generate a spatial random field on the mesh vertices by taking linear combinations of the Moran’s basis functions (contained in matrix \mathbf{M}) and their corresponding weights $\delta \in \mathbb{R}^p$. In Section 3.2, we

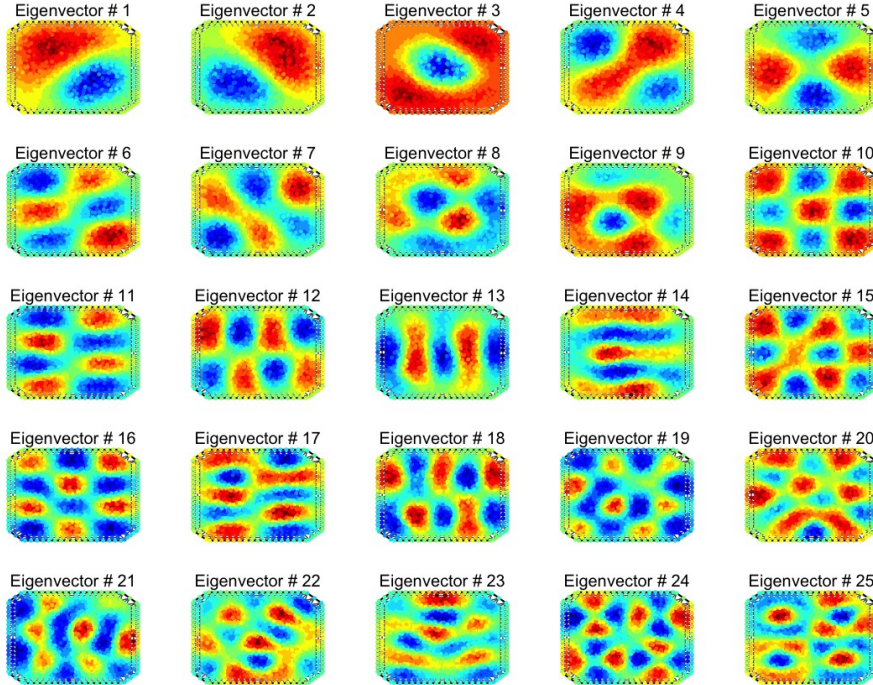


Figure 1: The leading 25 eigenvectors of the Moran’s operator generated on the triangular mesh. The distinct spatial patterns construct the latent spatial random field for hierarchical spatial models.

provide a general framework for estimating δ in hierarchical spatial models.

Piece-wise Linear Basis Functions

We introduce a set of piece-wise linear basis functions (Brenner and Scott, 2007) to interpolate points within the triangular mesh (i.e. the undirected graph $G = (V, E)$). We construct a spatial random field on the mesh nodes $\tilde{\mathbf{W}} = (W(v_1), \dots, W(v_m))$ where $v_i \in V$ and then project, or interpolate, onto the observed locations $\mathbf{W} = (W(s_1), \dots, W(s_n))$ where $s_i \in \mathcal{D}$. The latent spatial random field \mathbf{W} can be represented as $\mathbf{W} = \mathbf{A}\tilde{\mathbf{W}}$, where \mathbf{A} is an $n \times m$ projector matrix containing the piece-wise linear basis functions.

The rows of \mathbf{A} correspond to an observation location $s_i \in \mathcal{D}$, and the columns correspond to a mesh node $v_i \in V$. The i th row of \mathbf{A} contains the weights to linearly interpolate

$W(s_i)$. In practice, we use an $n \times m$ projector matrix \mathbf{A} for fitting the hierarchical spatial model. For model validation and prediction, we generate an $n_{CV} \times m$ projector matrix \mathbf{A}_{CV} that interpolates onto the validation locations.

The piece-wise linear basis functions can interpolate an observation location that is wholly contained in a triangle. Suppose point D is the observation location, points A , B , and C are the triangle vertices, and π_1, π_2 , and π_3 are the weights, where $\sum_i^3 \pi_i = 1$. π_1 is the proportion of the area of the triangle opposite of vertex A to the entire triangle. The same holds for values π_2 and π_3 with corresponding vertices B and C , respectively. We interpolate point D as the weighted mean of the three triangle vertices where $D \approx \pi_1 A + \pi_2 B + \pi_3 C$.

3.2 Bayesian Hierarchical Spatial Model using PICAR

In the previous section, we introduced three major components of PICAR: (1) the Moran’s basis function matrix $\mathbf{M} \in \mathbb{R}^{m \times p}$; (2) the projector matrix $\mathbf{A} \in \mathbb{R}^{n \times m}$; and (3) the corresponding weights $\delta \in \mathbb{R}^p$. Given a set of weights δ and the Moran’s basis functions \mathbf{M} , we can build a spatial random field on the triangular mesh nodes $v \in V$ as $\tilde{\mathbf{W}} = \mathbf{M}\delta$, where $\tilde{\mathbf{W}} = (W(v_1), \dots, W(v_m))$ for $v_i \in V$. Next, we linearly interpolate the latent spatial random field at the observation locations as $\mathbf{W} = \mathbf{A}\tilde{\mathbf{W}} = \mathbf{A}\mathbf{M}\delta$, where $\mathbf{W} = (W(s_1), \dots, W(s_n))$ for $s_i \in \mathcal{D}$, the spatial domain. An overview of these operations is provided in Figure 2.

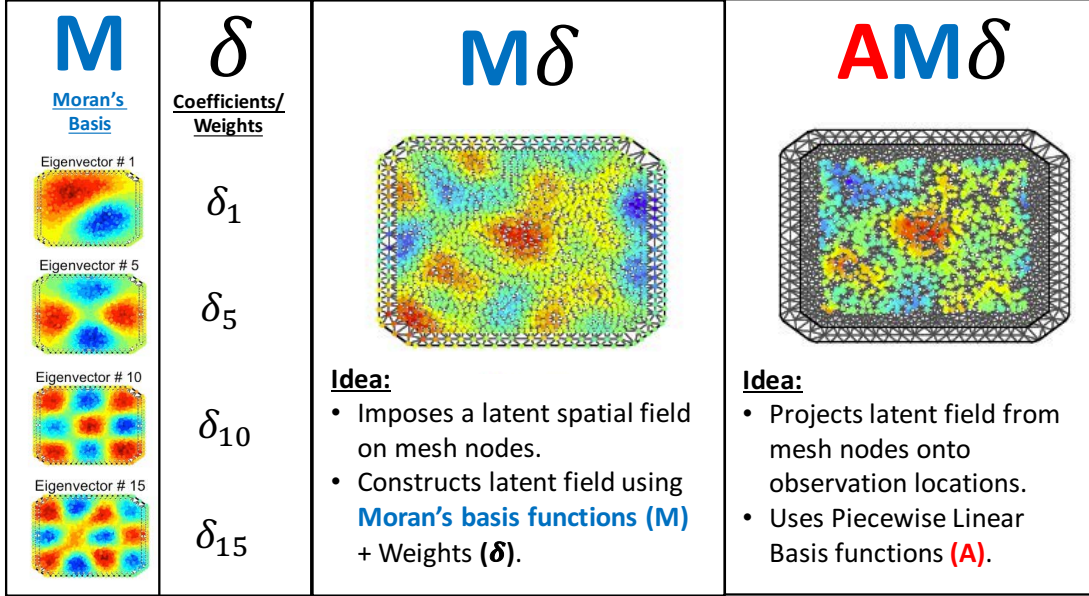


Figure 2: Diagram of the basis functions within PICAR. The Moran's basis functions (left) represent distinct spatial patterns, and the coefficients (δ) denote the associated weights. The operation $\mathbf{M}\delta$ constructs a latent field on the mesh nodes. The operation $\mathbf{A}\mathbf{M}\delta$ projects the mesh nodes onto the observation locations and generates a spatial random field.

PICAR can be embedded into the hierarchical spatial model framework:

$$\text{Data Model:} \quad Z(s)|\eta(s) \sim f(\eta(s)), \quad \eta(s) = g(E[Z(s)|\beta, \delta])$$

$$\boldsymbol{\eta} = (\eta(s_1), \dots, \eta(s_n)),$$

$$\boldsymbol{\eta} = \mathbf{X}\boldsymbol{\beta} + \mathbf{A}\mathbf{M}\boldsymbol{\delta},$$

$$\text{Process Model:} \quad \delta|\tau \sim \mathcal{N}(0, \tau^{-1}(\mathbf{M}'\mathbf{Q}\mathbf{M})^{-1}),$$

$$\text{Parameter Model:} \quad \boldsymbol{\beta} \sim N(\boldsymbol{\mu}_\beta, \boldsymbol{\Sigma}_\beta), \quad \tau \sim G(\alpha_\tau, \beta_\tau),$$

where \mathbf{A} is the projector matrix, \mathbf{M} is the Moran's basis functions matrix, δ are the basis coefficients, \mathbf{Q} is the prior precision matrix for the mesh vertices, τ is the precision parameter, and $\alpha_\tau, \beta_\tau, \boldsymbol{\mu}_\beta$, and $\boldsymbol{\Sigma}_\beta$ are the hyperparameters.

By default, we set \mathbf{Q} to be the precision matrix of an intrinsic conditional auto-regressive

model (ICAR) fit on the mesh vertices V . Here, $\mathbf{Q} = (\text{diag}(\mathbf{W}\mathbf{1}) - \mathbf{W})$, where \mathbf{W} is the adjacency or weight matrix from Section 3.1 and $\mathbf{1}$ is m -dimensional vector of 1s. Since \mathbf{Q} is not positive definite, this framework cannot be used within the likelihood function; however, it can be set as the prior distribution for the spatial random effects as part of the Bayesian hierarchical spatial model (Besag et al., 1991). We introduce alternative precision matrices in Section 3.3 and provide a comparative analysis across matrices in Section 4.

3.3 Automating PICAR

The traditional hierarchical spatial model (Section 2.1) assumes that the true latent spatial random field $\mathbf{W} = \{W(s_1), W(s_2), \dots, W(s_n)\}$ is a Gaussian process such that $\mathbf{W} \sim N(0, \sigma^2 R_\phi)$ with partial sill σ^2 and correlation matrix R_ϕ . On the other hand, PICAR considers the latent spatial random field following a basis representation such that $\mathbf{W} \approx \mathbf{A}\mathbf{M}\delta$, where $\delta \sim N(0, \tau^{-1}(\mathbf{M}'\mathbf{Q}\mathbf{M})^{-1})$, \mathbf{M} is the $m \times p$ Moran’s basis function matrix, and \mathbf{A} is the $n \times m$ projector matrix. An alternative formulation of the latent spatial random field is $\mathbf{W} \sim N(0, \tau^{-1}\mathbf{A}\mathbf{M}(\mathbf{M}'\mathbf{Q}\mathbf{M})^{-1}\mathbf{M}'\mathbf{A}')$.

Our objective is to accurately represent the the true latent state using PICAR’s basis representation. To that end, we can tune the rank of the Moran’s operator $\text{rank}(\mathbf{M})$ and the prior precision matrix \mathbf{Q} of the mesh vertices. The following automated heuristic selects an appropriate rank for the Moran’s basis. First, we generate a set \mathcal{P} consisting of h equally spaced points within the interval $[2, P]$ where P is the maximum rank and h is the interval resolution ($h = P - 1$ by default). Here, $P < m$ and both P and h are chosen by the user. For each $p \in \mathcal{P}$, we construct an $n \times (k + p)$ matrix of augmented

covariates $\tilde{X} = [X \quad \mathbf{A}\mathbf{M}_p]$ where $X \in \mathbb{R}^{n \times k}$ is the original covariate matrix, $\mathbf{A} \in \mathbb{R}^{n \times m}$ is the projector matrix, and $\mathbf{M}_p \in \mathbb{R}^{m \times p}$ are the leading p eigenvectors of the Moran’s operator. Next, we use maximum likelihood approaches to fit the appropriate generalized linear model (GLM) for the response type (e.g. binary, count, or ordered categorical). Finally, we select the rank p that yields the lowest out-of-sample cross-validated mean squared prediction error (CVMSPE).

Next, we provide some choices for \mathbf{Q} , the prior precision matrix for the mesh vertices $\tilde{\mathbf{W}}$. By default (Section 3.1), we set \mathbf{Q} to be the precision matrix of an intrinsic conditional auto-regressive model (ICAR). Similarly, we could set \mathbf{Q} as the precision matrix of a conditional auto-regressive model (CAR). Here, $\mathbf{Q} = (\text{diag}(\mathbf{W}\mathbf{1}) - \rho\mathbf{W})$, where \mathbf{W} is the adjacency matrix and $\rho \in (0, 1)$ is a predetermined correlation coefficient. It is possible to estimate ρ as a model parameter, but doing so requires an eigendecomposition of the Moran’s operator ($\mathcal{O}(m^3)$) at each iteration of the MCMC algorithm, which can negate the computational gains of PICAR. Another alternative is setting $\mathbf{Q} = I$, where the mesh nodes $\tilde{\mathbf{W}}$ and re-parameterized spatial random effects δ are uncorrelated.

3.4 Computational Gains

PICAR requires shorter computational times per iteration as well as fewer iterations for the Markov chain to converge. Computational speedup results from bypassing expensive matrix operations (e.g. Cholesky decomposition) and by decorrelating and reducing the dimensions of the spatial random effects. The computational cost is dominated by the matrix-vector multiplication $\mathbf{A}\mathbf{M}\delta$, where $\mathbf{A}\mathbf{M}$ is the $n \times p$ basis function matrix con-

structured prior to model fitting and δ are reparameterized spatial random effects (basis coefficients). PICAR has a computational complexity of $\mathcal{O}(np)$ as opposed to $\mathcal{O}(n^3)$ for the full hierarchical spatial model. Figure 3 illustrates the computational speedup offered by PICAR. As we increase the dimensionality of the observations n , the full hierarchical model quickly becomes computationally prohibitive. On the other hand, we can fit the model using PICAR within the order of minutes. The computation times are based on a single 2.2 GHz Intel Xeon E5-2650v4 processor. All the code was run on the Pennsylvania State University Institute for CyberScience-Advanced CyberInfrastructure (ICS-ACI) high-performance computing infrastructure.

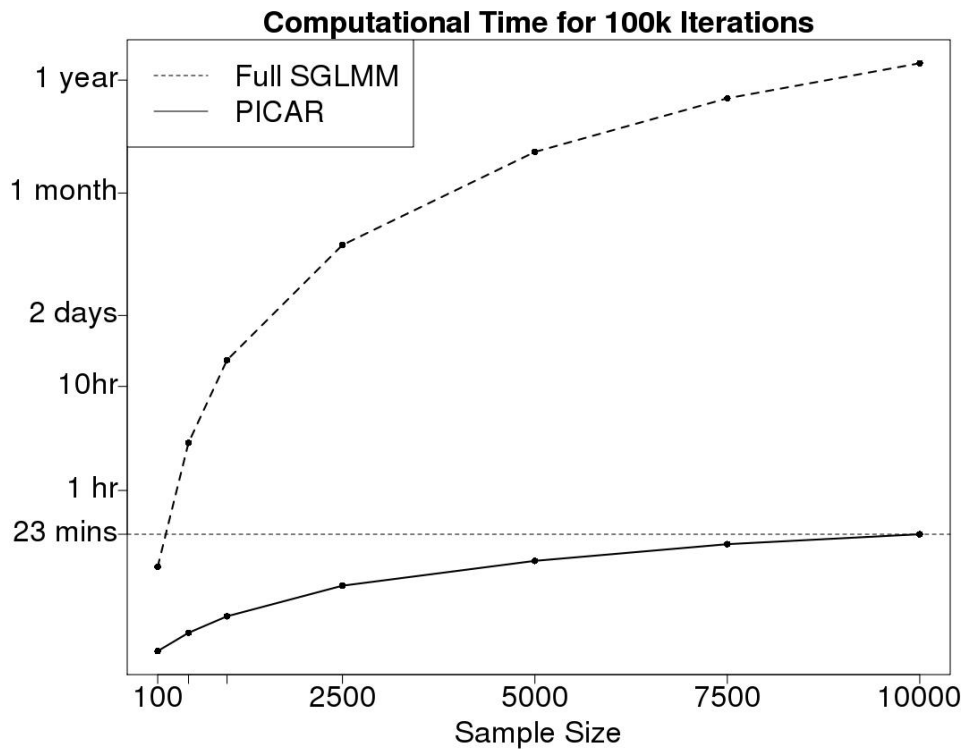


Figure 3: Computational time for 10^5 iterations versus sample size (n) for the full spatial generalized linear mixed model and PICAR with chosen rank $p = 50$.

PICAR results in a faster mixing MCMC algorithm than the reparameterized MCMC

algorithm (Rep-SGLMM) (Christensen et al., 2006), as shown by its larger effective sample size per second (ES/sec), the rate at which independent samples are generated by the MCMC algorithm. In the binary data example, the PICAR ES/s is roughly 345 times larger than the Rep-SGLMM approach (details in Section 4.1). We also show how to implement PICAR in the `stan` programming language (Carpenter et al., 2017), which generates a fast mixing MCMC algorithm based on a specified model.

For PICAR, the two major computational bottlenecks are constructing the Moran’s operator (Section 3.1) and computing its eigencomponents. The Moran’s operator requires the matrix operation $(\mathbf{I} - \mathbf{1}\mathbf{1}'/m)\mathbf{W}(\mathbf{I} - \mathbf{1}\mathbf{1}'/m)$ and $2m^3 - m^2$ floating point operations (flops), which may be computationally prohibitive for large datasets. We reduce computational costs by leveraging the embarrassingly parallel operations as well the sparsity of the weights matrix \mathbf{W} .

We can compute the k eigencomponents of the Moran’s Operator using a partial eigendecomposition approach such as the Implicitly Restarted Arnoldi Method (Lehoucq et al., 1998) from `RSpectra` package (Qiu and Mei, 2019). Since PICAR typically selects a $\text{rank}(\mathbf{M}) \ll m$, it is not necessary to perform a full eigendecomposition.

4 Simulation Study

We study PICAR via simulation studies in several hierarchical spatial models: (i) a binary spatial generalized linear mixed model shows that our approach produces similar results to fitting the full (“gold standard”) spatial model; (ii) a spatially varying coefficients model demonstrates how PICAR can be easily extended to user-specified models using the lan-

guage `stan`; (iii) an ordered categorical data example shows how our approach is efficient for a problem for which other methods are not readily applicable.

4.1 Binary Data

We generate 100 datasets with randomly chosen locations on $[0, 1]^2$. Each dataset consists of 1,400 locations with 1,000 for model fitting and 400 for validation. We chose $n = 1,000$ to enable comparisons with fitting the full spatial model. We compare PICAR’s performance across varying ranks of the Moran’s operator $p = \{10, 50, 75, 100, 200\}$. We also compare three different precision matrices, Independent, ICAR, and CAR with the rank chosen by our heuristic (Section 3.3). The CAR precision matrix uses a correlation parameter $\rho = 0.5$ to select the rank. We compare PICAR’s inference and prediction performance against a gold standard approach that uses the fast mixing MCMC algorithm in Christensen et al. (2006). We set $\beta = (1, 1)^T$, covariance function parameters $\nu = 2.5$, $\sigma^2 = 1$, and $\phi = 0.2$. We set priors following Hughes and Haran (2013): $\beta \sim N(\mathbf{0}, 100I)$, $\tau \sim G(0.5, 2000)$.

For PICAR, we use a triangular mesh with $m = 1,649$ vertices. For the binary and count data, we use Gibbs updates for τ and random-walk Metropolis-Hastings updates for β with proposal $\beta^{(i+1)} \sim N(\beta^{(i)}, \hat{\mathbf{V}})$, where $\hat{\mathbf{V}}$ is the asymptotic covariance matrix from fitting the classical generalized linear model. Finally, we update the reparameterized random effects δ using an all-at-once normal random walk Metropolis-Hastings update (Guan and Haran, 2018). For PICAR we ran 300,000 iterations of the MCMC algorithm.

We model spatial binary observations generated via the logit-link function $\text{logit}(p) = \log\{\frac{p}{1-p}\}$. We select one sample (from the 100 generated samples) as the dataset for the

comparative analysis. When comparing across ranks, we use the precision matrix from the ICAR model $\mathbf{Q} = (\text{diag}(\mathbf{W}\mathbf{1}) - \mathbf{W})$. We examine the out-of-sample cross-validated mean squared prediction error $\text{CVMSPE} = \frac{1}{n_{CV}} \sum_{i=1}^{n_{CV}} (Y_i^* - \hat{Y}_i^*)^2$, where $n_{CV} = 400$, Y_i^* 's denote the i -th value in the validation sample, and \hat{Y}_i^* 's are the predicted values at the i -th location.

Table 1 presents the parameter estimates, prediction results, and computational times for each rank p of the Moran's Operator. Results suggest that the rank is a key driver for predictive performance and parameter estimation. PICAR is not sensitive to the chosen precision matrix \mathbf{Q} , as the results are similar across precision matrices. PICAR improves mixing in the MCMC algorithm as shown by the larger effective samples per second (ES/sec) compared to the gold standard approach. For model parameters β_1 and β_2 , PICAR yields an ES/sec of 29.4 and 40.2 respectively and the gold standard returns an ES/sec 0.19 and 0.29 respectively. For the random effects \mathbf{W} , the average ES/sec is 5.8 for the PICAR approach and 0.016 for the gold standard, an improvement by a factor of roughly 345.

Rank	β_1 (95% CI)	β_2 (95% CI)	CVMPSE	Time (min)
10	1.04 (0.77,1.31)	0.91 (0.64,1.16)	0.3	9.73
22	1.09 (0.82,1.37)	0.93 (0.67,1.2)	0.27	10.73
50	1.12 (0.83,1.41)	0.95 (0.67,1.23)	0.28	11.14
75	1.14 (0.85,1.44)	0.98 (0.69,1.26)	0.28	11.62
100	1.2 (0.9,1.5)	1 (0.71,1.29)	0.29	12.28
200	1.34 (1.01,1.66)	0.99 (0.69,1.31)	0.32	15.13
Gold Standard	1.03 (0.77,1.3)	0.89 (0.63,1.16)	0.29	3624.43

Table 1: Simulated example with binary spatial observations. Parameter estimation, prediction, and model fitting time results across Moran's basis ranks. Bold font denotes the rank chosen by the automated heuristic.

Note that the PICAR approach is computationally efficient, and it also outperforms

the gold standard approach in prediction. This is consistent with results from another basis representation approach, the latent conjugate model (Bradley et al., 2019), which also outperforms the full SGLMM in computational cost and predictive ability. This may be attributed to the flexibility of PICAR’s basis representation of the latent spatial field.

We examine boxplots for the parameter estimates of β_1 and β_2 across the 100 samples (Supplement). The point estimates from the PICAR approach are distributed narrowly around the true values. The distribution of the point estimates remain similar across the choice of precision matrix \mathbf{Q} . The coverage proportions (0.89 for β_1 , 0.91 for β_2) are close to but lower than the nominal coverage value (0.95).

4.2 Poisson Data with Spatially Varying Coefficients

We incorporate the PICAR approach to the spatially varying coefficients model using the `stan` programming language (Carpenter et al., 2017), a popular computing framework for Bayesian inference. As in the binary example, we generate $n = 1,400$ observations using the model parameters β and ϕ as in the binary case. We assign one set of spatially varying coefficients $\beta_1(s)$ corresponding to the first covariate X_1 . $\mathbf{W} = (w(s_1), \dots, w(s_n))$ are the spatial random effects and $\mathbf{B} = (\beta_1(s_1), \dots, \beta_1(s_n))$ is the n -dimensional vector of the spatially varying coefficients for locations $s_i \in \mathcal{D}$. Here, $(\mathbf{W}, \mathbf{B})^T \sim \mathcal{N}(0, \mathcal{N}(\mathbf{0}, R_\phi \otimes \mathbf{T}))$, where R_ϕ is the correlation function from the binary case and $\mathbf{T} = \begin{bmatrix} 1.0 & 0.3 \\ 0.3 & 0.2 \end{bmatrix}$. In the PICAR framework, we represent the spatial processes \mathbf{B} and \mathbf{W} by $\mathbf{B} \approx \mathbf{A}\mathbf{M}\delta_\beta$ and $\mathbf{W} \approx \mathbf{A}\mathbf{M}\delta_w$, where \mathbf{A} is the $n \times m$ projector matrix, \mathbf{M} is the $m \times p$ Moran’s basis function matrix, and δ_β and δ_w are the corresponding $p \times 1$ basis coefficients. Note that

we are modeling both spatial process \mathbf{B} and \mathbf{W} as independent spatial processes with no cross-correlations. The PICAR specification of this hierarchical model is as follows:

$$\begin{aligned}
\text{Data Model:} \quad & Z(s)|\eta(s) \sim f(\eta(s)), \quad \eta(s) = g(\mathbb{E}[Z(s)|\beta, \delta_\beta, \delta_w]), \\
& \boldsymbol{\eta} = \mathbf{X}\beta + X_1\mathbf{A}\mathbf{M}\delta_\beta + \mathbf{A}\mathbf{M}\delta_w, \text{ where } \boldsymbol{\eta} = (\eta(s_1), \dots, \eta(s_n)), \\
\text{Process Model:} \quad & \delta_\beta \sim \mathcal{N}(0, \tau_\beta^{-1}(\mathbf{M}'\mathbf{Q}_\beta\mathbf{M})^{-1}), \quad \delta_w \sim \mathcal{N}(0, \tau_w^{-1}(\mathbf{M}'\mathbf{Q}_w\mathbf{M})^{-1}) \\
\text{Parameter Model:} \quad & \tau_\beta \sim G(\alpha_{\tau_1}, \beta_{\tau_1}), \quad \tau_w \sim G(\alpha_{\tau_2}, \beta_{\tau_2}), \quad \beta \sim N(\mu_\beta, \Sigma_\beta),
\end{aligned}$$

where X_1 is the first column of the $n \times 2$ design matrix \mathbf{X} . \mathbf{Q}_β and \mathbf{Q}_w are the $m \times m$ precision matrix for the mesh vertices and τ_β and τ_w are the precision parameters. $\alpha_{\tau_1}, \beta_{\tau_1}, \alpha_{\tau_2}, \beta_{\tau_2}, \mu_\beta$, and Σ_β are the hyperparameters. Note that the p -dimensional vectors δ_β and δ_w replace the n -dimensional vectors \mathbf{B} and \mathbf{W} in the original model.

We compare PICAR's performance across varying ranks $p = \{10, 50, 63, 75, 100, 200\}$ for the Moran's operator. The lowest CVMSPE is achieved when we use the rank ($p = 63$) selected via our automated heuristic. Model fitting times increase with respect to the chosen rank of the Moran's operator. Using `stan`, we obtained a fast mixing MCMC algorithm, and an effective sample size of $\sim 5,000$ for all parameters, random effects $w(s)$, and the spatially varying coefficients $\beta(s)$.

4.3 Ordered Categorical Data

Let $Z(s)$ be the observation at $s \in \mathcal{D}$ with J ordered categories. We model ordered categorical data using the spatial cumulative-logit model through PICAR as follows:

$$\begin{aligned}
\textbf{Data Model:} \quad & Z(s)|\boldsymbol{\gamma}(s) \sim f(\boldsymbol{\gamma}(s)), \quad \boldsymbol{\gamma}(s) = (\gamma_1(s), \dots, \gamma_J(s)) \\
& \gamma_j(s)|\beta, \theta, \delta = \frac{\exp\{\theta_j - (\mathbf{X}(s)\beta + [\mathbf{AM}\delta](s))\}}{1 + \exp\{\theta_j - (\mathbf{X}(s)\beta + [\mathbf{AM}\delta](s))\}} \\
& \theta_j|\alpha = \sum_{i=1}^{J-1} \exp\{\alpha_i\} \\
\textbf{Process Model:} \quad & \delta|\tau \sim \mathcal{N}(0, \tau^{-1}(\mathbf{M}'\mathbf{Q}\mathbf{M})^{-1}), \\
\textbf{Parameter Model:} \quad & \alpha \sim p(\alpha), \quad \beta \sim N(\mu_\beta, \Sigma_\beta), \quad \tau \sim G(\alpha_\tau, \beta_\tau),
\end{aligned}$$

where γ_j and θ_j are the cumulative probability and intercept (“cutoff”) for the j -th category, respectively. \mathbf{A} is the $n \times m$ projector matrix, \mathbf{M} is the $m \times p$ Moran’s basis function matrix, δ is the $p \times 1$ vector of random effects, and μ_β , Σ_β , α_τ , and β_τ are hyperparameters.

We fix the first cutoff $\theta_1 = 0$ to avoid identifiability issues (Johnson and Albert, 2006). Note that the θ_j ’s are constrained by the ordering $\theta_j > \theta_k$ for $j > k$. Through a transformation (Higgs and Hoeting, 2010; Albert and Chib, 1997), we can generate unconstrained cutoff parameters $\alpha = (\alpha_1, \alpha_2, \dots, \alpha_{J-1})$, where $\alpha_1 = -\infty$, $\alpha_2 = \log(\theta_2)$, and $\alpha_3 = \log(\theta_3 - \theta_2)$. The inverse transformation is $\theta_j = \sum_{i=1}^{J-1} \exp\{\alpha_i\}$.

Similar to the binary case, we generate 100 samples, one of these samples is used for our comparative analysis. The true cut-off parameters are $\theta_1 = 0$, $\theta_2 = 1$ and $\theta_3 = 2$. The other model parameters are similar to that in the binary case. To assess predictive performance, we examine the out-of-sample misprediction rate (MPR), or the proportion of incorrect predictions, and the loss function is $\text{MPR} = \frac{1}{n_{CV}} \sum_{i=1}^{n_{CV}} I_{(Y_i^* \neq \hat{Y}_i^*)}$, where \hat{Y}^* are the predicted values and Y^* are the true values at the validation locations. The automated heuristic chose

a rank of $p = 23$, which yields comparable parameter estimation and predictive ability to the gold standard. Predictive ability does not vary considerably across rank, but rank impacts parameter estimation. PICAR is not sensitive to the chosen precision matrix Q , as the inferential and predictive performances do not vary across precision matrices. Similar to the binary case, we observe faster mixing with the PICAR approach: for β_1 and β_2 , PICAR has an ES/sec of 30.7 and 30.4, while the gold standard has an ES/sec 0.034 and 0.034 respectively. For the random effects, PICAR has an average ES/sec of 4.4 versus 0.003 for the gold standard, a factor of around 1,487. For the simulation study, we examine boxplots for the parameter estimates for β_1 , β_2 , α_1 , and α_2 across all 100 samples. Similar to the binary case, our coverage proportions are very close (0.91 for β_1 , 0.92 for β_2 , 0.93 for α_1 , 0.88 for α_2), but slightly lower than the nominal coverage (0.95).

5 Real Data Examples

We demonstrate how PICAR scales well to high-dimensional spatial datasets.

5.1 Binary Data: Parasitic Infestation of Dwarf Mistletoe

In Minnesota, the eastern spruce dwarf mistletoe (*Arceuthobium pusillum*) are a parasitic species that affect the longevity and quality of its host, the black spruce (*Picea mariana*) (Geils and Hawksworth, 2002). We use data from the Minnesota Department of Natural Resources (DNR) forest inventory (cf. Hanks et al., 2011). The response is a binary incidence of dwarf mistletoe at $n = 25,431$ black spruce stands (location hosting the black spruce samples). We randomly sample 22,888 observations to fit our model and reserve

2,543 observations for validation. Covariates include: (1) average age of trees in the stand; (2) basal area per acre of trees in the stand; (3) average canopy height; and (4) volume of the stand in cords, a unit of measurement. We fit the binary spatial model of Section 4.1 and construct a triangular mesh with $m = 32,611$ vertices, using our heuristic (Section 3.3) to select a rank of $p = 520$ for the Moran’s basis functions matrix.

The PICAR approach required around 4 hours: 2 hours to run 10^5 iterations of the MCMC algorithm, 10 minutes to generate the Moran’s operator (Section 3.1) via parallel computing across 100 processors, and 1.7 hours to calculate the first 1,000 eigencomponents using the **Spectra** C++ library. Comparison with the full SGLMM is computationally infeasible. The posterior predictive map displays similar spatial patterns between the predicted values and the validation sample.

5.2 Ordered Categorical Data: Maryland Stream Waders

Beginning as a pilot program in 2000, the Maryland Stream Waders (MSW) program is a statewide volunteer stream monitoring program managed by the Maryland Department of Natural Resources (DNR) and the Monitoring and Non-Tidal Assessment Division (MANTA). For each sample, the DNR laboratory calculated a Benthic Index of Biotic Integrity (BIBI) was calculated (on a 1 to 5 scale). Each site was rated either Good (4-5), Fair (3-3.9), or Poor (1-2.9) (Stribling et al., 1998). A total of 6,951 samples were collected within a 17-year time period (2000-2017) at irregular sampling locations (Maryland’s Mapping and GIS Data Portal, 2018). We fit the model using 5,561 randomly selected observations and validate the model with the remaining 1,390 samples. We fit

a spatial cumulative-logit model with just an intercept term. We generated a mesh with $m = 8,810$ nodes and the automated heuristic chose a rank of $p = 653$. The time to fit the spatial cumulative-logit model via PICAR is around 35 minutes. We estimate fitting the full model would require on the order of weeks to provide similarly accurate inference.

6 Discussion

In this study, we propose a fast extendable projection-based approach (PICAR) for modeling a wide range of hierarchical spatial models. In cases where it is possible to fit the full hierarchical spatial model, we show that our approach yields comparable results in terms of both inference and prediction. We also provide a variety of other examples that illustrate the flexibility of the PICAR approach as well as the ease with which non-experts can specify and efficiently fit their own hierarchical spatial models. We show that our approach is computationally efficient, scales up to higher dimensions, automated, and extendable to a variety of hierarchical spatial models. We provide an example of a hierarchical spatial model (ordinal spatial data) that cannot be fit using existing publicly available code but can be easily fit using PICAR. Moreover, we show that our approach is amenable to implementation in a programming language for Bayesian inference (`stan`). As shown in our real-data applications, our approach scales well to higher dimensions. Where other approaches may be computationally infeasible, we can fit a high-dimensional hierarchical spatial model within hours.

The computational complexity for the PICAR approach is driven by matrix-vector multiplications, which can be readily parallelized. With efficient parallelization methods,

we expect our approach to scale up to hundreds of thousands of data points. Even though an eigendecomposition is only carried out once in our approach, methods such as Nyström method (Williams and Seeger, 2001) or random projections (Banerjee et al., 2013; Guan and Haran, 2018) can further reduce costs via an approximate eigendecomposition of the Moran’s operator. There may be other methods to improve our automated heuristic for rank selection such as implementing a screening process for the relevant basis functions via a variable selection approach like LASSO (Tibshirani, 1994). Extending the PICAR approach to spatio-temporal or multivariate spatial processes as well as computer model calibration with non-Gaussian model outputs may provide fruitful avenues for future research.

7 Acknowledgments

We are grateful to Ephraim Hanks, Erin Schliep, Yawen Guan, Jaewoo Park, and Klaus Keller for helpful discussions. This work was partially supported by the U.S. Department of Energy, Office of Science, Biological and Environmental Research Program, Earth and Environmental Systems Modeling, MultiSector Dynamics, Contract No. DE-SC0016162 and by the National Science Foundation through the Network for Sustainable Climate Risk Management (SCRiM) under NSF cooperative agreement GEO-1240507. This study was also co-supported by the Penn State Center for Climate Risk Management. Any opinions, findings, and conclusions or recommendations expressed in this material are those of the authors and do not necessarily reflect the views of the Department of Energy, the National Science Foundation, or other funding entities. Any errors and opinions are those of the authors. We are not aware of any real or perceived conflicts of interest for any authors.

SUPPLEMENTARY MATERIAL

Supplemental Tables and Figures: Additional figures and tables for the simulation study, the dwarf mistletoe study, and the Maryland Stream Waders application (.pdf file)

Dwarf mistletoe data set: Data set used in the dwarf mistletoe application (Section 5.1. (.txt file)

Maryland Stream Waders data set: Data set used in the Maryland Stream Waders application (Section 5.2). (.txt file)

References

Albert, J. H. and Chib, S. (1993). Bayesian analysis of binary and polychotomous response data. *Journal of the American statistical Association*, 88(422):669679.

Albert, J. H. and Chib, S. (1997). Bayesian methods for cumulative, sequential, and two-step ordinal data regression models. Technical report, Bowling Green State University.

Banerjee, A., Dunson, D. B., and Tokdar, S. T. (2013). Efficient Gaussian process regression for large datasets. *Biometrika*, 100(1):7589.

Banerjee, S., Carlin, B. P., and Gelfand, A. E. (2014). *Hierarchical modeling and analysis for spatial data*. Chapman and Hall/CRC.

Banerjee, S., Gelfand, A. E., Finley, A. O., and Sang, H. (2008). Gaussian predictive

- process models for large spatial data sets. *Journal of the Royal Statistical Society: Series B (Statistical Methodology)*, 70(4):825–848.
- Bernardinelli, L., Pascutto, C., Best, N., and Gilks, W. (1997). Disease mapping with errors in covariates. *Statistics in Medicine*, 16(7):741–752.
- Besag, J., York, J., and Mollié, A. (1991). Bayesian image restoration, with two applications in spatial statistics. *Annals of the institute of statistical mathematics*, 43(1):1–20.
- Bradley, J. R., Cressie, N., Shi, T., et al. (2016). A comparison of spatial predictors when datasets could be very large. *Statistics Surveys*, 10:100–131.
- Bradley, J. R., Holan, S. H., and Wikle, C. K. (2019). Bayesian hierarchical models with conjugate full-conditional distributions for dependent data from the natural exponential family. *Journal of the American Statistical Association*, 0(ja):1–29.
- Brenner, S. and Scott, R. (2007). *The mathematical theory of finite element methods*, volume 15. Springer Science & Business Media.
- Carpenter, B., Gelman, A., Hoffman, M. D., Lee, D., Goodrich, B., Betancourt, M., Brubaker, M., Guo, J., Li, P., and Riddell, A. (2017). Stan: A probabilistic programming language. *Journal of statistical software*, 76(1).
- Christensen, O. F., Roberts, G. O., and Sköld, M. (2006). Robust Markov chain Monte Carlo methods for spatial generalized linear mixed models. *Journal of Computational and Graphical Statistics*, 15(1):1–17.

- Cressie, N. and Johannesson, G. (2008). Fixed rank kriging for very large spatial data sets. *Journal of the Royal Statistical Society: Series B (Statistical Methodology)*, 70(1):209–226.
- Datta, A., Banerjee, S., Finley, A. O., and Gelfand, A. E. (2016). Hierarchical nearest-neighbor Gaussian process models for large geostatistical datasets. *Journal of the American Statistical Association*, 111(514):800–812.
- De Oliveira, V. (2000). Bayesian prediction of clipped Gaussian random fields. *Computational Statistics & Data Analysis*, 34(3):299–314.
- Diggle, P. J., Tawn, J. A., and Moyeed, R. (1998). Model-based geostatistics. *Journal of the Royal Statistical Society: Series C (Applied Statistics)*, 47(3):299–350.
- Furrer, R., Genton, M. G., and Nychka, D. (2006). Covariance tapering for interpolation of large spatial datasets. *Journal of Computational and Graphical Statistics*, 15(3):502–523.
- Geils, B. and Hawksworth, F. (2002). Damage, effects, and importance of dwarf mistletoes. *In: Geils, Brian W.; Cibrián Tovar, Jose; Moody, Benjamin, tech. coords. Mistletoes of North American Conifers. Gen. Tech. Rep. RMRS-GTR-98. Ogden, UT: US Department of Agriculture, Forest Service, Rocky Mountain Research Station. p. 57-65, 98.*
- Gelfand, A. E., Kim, H.-J., Sirmans, C., and Banerjee, S. (2003). Spatial modeling with spatially varying coefficient processes. *Journal of the American Statistical Association*, 98(462):387–396.

- Griffith, D. A. (2003). Spatial filtering. In *Spatial Autocorrelation and Spatial Filtering*, pages 91–130. Springer.
- Guan, Y. and Haran, M. (2018). A computationally efficient projection-based approach for spatial generalized linear mixed models. *Journal of Computational and Graphical Statistics*, 27(4):701714.
- Guan, Y. and Haran, M. (2019). Fast expectation-maximization algorithms for spatial generalized linear mixed models. *arXiv preprint arXiv:1909.05440*.
- Guhaniyogi, R., Finley, A. O., Banerjee, S., and Gelfand, A. E. (2011). Adaptive Gaussian predictive process models for large spatial datasets. *Environmetrics*, 22(8):997–1007.
- Hanks, E. M., Hooten, M. B., and Baker, F. A. (2011). Reconciling multiple data sources to improve accuracy of large-scale prediction of forest disease incidence. *Ecological Applications*, 21(4):1173–1188.
- Haran, M., Hodges, J. S., and Carlin, B. P. (2003). Accelerating computation in markov random field models for spatial data via structured MCMC. *Journal of Computational and Graphical Statistics*, 12(2):249–264.
- Heaton, M. J., Datta, A., Finley, A. O., Furrer, R., Guinness, J., Guhaniyogi, R., Gerber, F., Gramacy, R. B., Hammerling, D., Katzfuss, M., et al. (2019). A case study competition among methods for analyzing large spatial data. *Journal of Agricultural, Biological and Environmental Statistics*, 24(3):398–425.

- Higdon, D. (1998). A process-convolution approach to modelling temperatures in the North Atlantic Ocean. *Environmental and Ecological Statistics*, 5(2):173–190.
- Higgs, M. D. and Hoeting, J. A. (2010). A clipped latent variable model for spatially correlated ordered categorical data. *Computational Statistics & Data Analysis*, 54(8):1999–2011.
- Hjelle, Ø. and Dæhlen, M. (2006). *Triangulations and applications*. Springer Science & Business Media.
- Hughes, J. and Haran, M. (2013). Dimension reduction and alleviation of confounding for spatial generalized linear mixed models. *Journal of the Royal Statistical Society: Series B (Statistical Methodology)*, 75(1):139–159.
- Johnson, V. E. and Albert, J. H. (2006). *Ordinal data modeling*. Springer Science & Business Media.
- Katzfuss, M. (2017). A multi-resolution approximation for massive spatial datasets. *Journal of the American Statistical Association*, 112(517):201–214.
- Lehoucq, R. B., Sorensen, D. C., and Yang, C. (1998). *ARPACK users' guide: solution of large-scale eigenvalue problems with implicitly restarted Arnoldi methods*, volume 6. Siam.
- Lindgren, F., Rue, H., et al. (2015). Bayesian spatial modelling with R-INLA. *Journal of Statistical Software*, 63(19):1–25.

- Lindgren, F., Rue, H., and Lindström, J. (2011). An explicit link between Gaussian fields and Gaussian Markov random fields: the stochastic partial differential equation approach. *Journal of the Royal Statistical Society: Series B (Statistical Methodology)*, 73(4):423–498.
- Maryland’s Mapping and GIS Data Portal (2018). Maryland Stream Health - Stream Wader Sites volunteer collected. Data retrieved from MD iMAP, https://geodata.md.gov/imap/rest/services/Hydrology/MD_StreamHealth/FeatureServer/0.
- Moran, P. A. (1950). Notes on continuous stochastic phenomena. *Biometrika*, 37(1/2):17–23.
- Mu, J., Wang, G., and Wang, L. (2018). Estimation and inference in spatially varying coefficient models. *Environmetrics*, 29(1):e2485.
- Muff, S., Riebler, A., Held, L., Rue, H., and Saner, P. (2015). Bayesian analysis of measurement error models using integrated nested Laplace approximations. *Journal of the Royal Statistical Society: Series C (Applied Statistics)*, 64(2):231–252.
- Nychka, D., Bandyopadhyay, S., Hammerling, D., Lindgren, F., and Sain, S. (2015). A multiresolution Gaussian process model for the analysis of large spatial datasets. *Journal of Computational and Graphical Statistics*, 24(2):579–599.
- Park, J. and Haran, M. (2019). Reduced-dimensional monte carlo maximum likelihood for latent gaussian random field models. *arXiv preprint arXiv:1910.09711*.

- Qiu, Y. and Mei, J. (2019). *RSpectra: Solvers for Large-Scale Eigenvalue and SVD Problems*. R package version 0.15-0.
- Rue, H., Martino, S., and Chopin, N. (2009). Approximate Bayesian inference for latent Gaussian models by using integrated nested Laplace approximations. *Journal of the royal statistical society: Series b (statistical methodology)*, 71(2):319–392.
- Sengupta, A. and Cressie, N. (2013). Hierarchical statistical modeling of big spatial datasets using the exponential family of distributions. *Spatial Statistics*, 4:14–44.
- Sengupta, A., Cressie, N., Kahn, B. H., and Frey, R. (2016). Predictive inference for big, spatial, non-Gaussian data: MODIS cloud data and its change-of-support. *Australian & New Zealand Journal of Statistics*, 58(1):15–45.
- Stein, M. L. (2012). *Interpolation of spatial data: some theory for kriging*. Springer Science & Business Media.
- Stein, M. L. (2013). Statistical properties of covariance tapers. *Journal of Computational and Graphical Statistics*, 22(4):866–885.
- Stribling, J. B., Jessup, B. K., White, J. S., Boward, D., and Hurd, M. (1998). Development of a benthic index of biotic integrity for Maryland streams. *CBWP-MANTA EA-98-3 Maryland Department of Natural Resources, Annapolis, Maryland*.
- Sun, Y., Li, B., and Genton, M. G. (2012). Geostatistics for large datasets. In *Advances and Challenges in Space-Time Modelling of Natural Events*, pages 55–77. Springer.

- Tibshirani, R. (1994). Regression shrinkage and selection via the lasso. *Journal of the Royal Statistical Society, Series B*, 58:267–288.
- Wikle, C. K., Berliner, L. M., and Cressie, N. (1998). Hierarchical Bayesian space-time models. *Environmental and Ecological Statistics*, 5(2):117–154.
- Williams, C. and Seeger, M. (2001). Using the Nyström method to speed up kernel machines. In *Advances in Neural Information Processing Systems 13*, pages 682–688. MIT Press.
- Xia, H. and Carlin, B. P. (1998). Spatio-temporal models with errors in covariates: Mapping Ohio lung cancer mortality. *Statistics in Medicine*, 17(18):2025–2043.

Supplemental Information for “PICAR: An Efficient Extendable Approach for Fitting Hierarchical Spatial Models”

1 Examples of Hierarchical Spatial Models

Here we provide examples of hierarchical spatial models. The first is the class of spatial generalized linear mixed models for non-Gaussian data, the second is a spatially varying coefficient model, and the third is a cumulative-logit model for ordered categorical data.

Spatial Generalized Linear Mixed Models

Non-Gaussian spatial observations are typically modeled using spatial generalized linear mixed models (SGLMMs) (Diggle et al., 1998, Haran, 2011). Let $\{Z(s) : s \in \mathcal{D}\}$ be a non-Gaussian spatial random field. Assuming $Z(s)$ are conditionally independent given the latent random spatial field \mathbf{W} , the conditional mean $E[Z(s)|\beta, \mathbf{W}, \epsilon(s)]$ can be modeled through a linear predictor $\eta(s)$:

$$\eta(s) = g\{E[Z(s)|\beta, \mathbf{W}], \epsilon(s)\} = X(s)\beta + w(s) + \epsilon(s),$$

where $g(\cdot)$ is a known link function. Binary and count observations are two common types of non-Gaussian spatial data, and these can be modeled using the binary SGLMM with logit link and the Poisson SGLMM with log link, respectively.

The general Bayesian hierarchical framework for non-Gaussian spatial observations is:

$$\begin{aligned}
\text{Data Model:} \quad & Z(s)|\eta(s) \sim f(\eta(s)) \\
& \eta(s) = g(\mathbb{E}[Z(s)|\beta, \mathbf{W}], \epsilon(s)) = X(s)\beta + w(s) + \epsilon(s) \\
\text{Process Model:} \quad & \mathbf{W}|\phi, \sigma^2 \sim N(0, \sigma^2 R_\phi) \\
& \epsilon(s)|\tau^2 \sim N(\mathbf{0}, \tau^2) \\
\text{Parameter Model:} \quad & \beta \sim p(\beta), \phi \sim p(\phi), \sigma^2 \sim p(\sigma^2), \tau^2 \sim p(\tau^2)
\end{aligned}$$

Spatially Varying Coefficient Models

Spatially varying coefficient models (Gelfand et al., 2003) consider cases where the fixed effects β vary across space. For the case with a single predictor $X(s)$, the data model is $Z(s) = \beta_0 + \beta_1 X(s) + \beta_1(s)X(s) + w(s) + \epsilon(s)$, where β_0 is the intercept, β_1 is the fixed effect, $\beta_1(s)$ is the spatially varying coefficient term, and $w(s)$ and $\epsilon(s)$ are the spatial random effects and micro-scale measurement errors, respectively. Here, $\mathbf{B} = (\beta_1(s_1), \dots, \beta_1(s_n))$ is the n -dimensional vector of spatially varying coefficients, and $\mathbf{B} \sim N(0, \sigma_\beta^2 R_{\phi_\beta})$ where σ_β^2 is the partial sill and ϕ_β is the range parameter for the spatial random process \mathbf{B} .

For cases with k predictors, we have the following hierarchical spatial model:

$$\begin{aligned}
\text{Data Model:} \quad & Z(s)|\eta(s) \sim f(\eta(s)) \\
& \eta(s) = g(\mathbb{E}[Z(s)|\beta, \mathbf{B}, \mathbf{W}, \epsilon(s)]) = X(s)\beta + X(s)\beta(s) + w(s) + \epsilon(s) \\
\text{Process Model:} \quad & (\mathbf{W}, \mathbf{B})^T|\phi, \mathbf{T} \sim \mathcal{N}(\mathbf{0}, R_\phi \otimes \mathbf{T}) \\
& \epsilon(s)|\tau^2 \sim N(\mathbf{0}, \tau^2) \\
\text{Parameter Model:} \quad & \beta \sim \pi(\beta), \quad \tau^2 \sim \pi(\tau^2), \quad \phi \sim \pi(\phi), \quad \mathbf{T} \sim \pi(\mathbf{T})
\end{aligned}$$

where β is the k -dimensional vector of the fixed effects, $\beta(s) = (\beta_1(s), \dots, \beta_k(s))$ is a k -dimensional vector of the spatially varying coefficients for location s , $\mathbf{B} = (\beta(s_1), \dots, \beta(s_n))$ is the nk -dimensional vector of all spatially varying coefficients, $\mathbf{W} = (W(s_1), \dots, W(s_n))$

is the n -dimensional vector of the spatial random effects, R_ϕ and τ^2 are the correlation matrix and nugget variance, and \mathbf{T} is a $(k+1) \times (k+1)$ positive definite matrix.

Cumulative-Logit Models for Ordinal Spatial Data

Ordered categorical (ordinal) data are categorical responses with a natural ordering, and commonly used in survey questionnaires, patient responses in clinical trials, and quality assurance ratings for industrial processes. (Higgs and Hoeting, 2010; Schliep and Hoeting, 2013) develop a hierarchical spatial model for ordinal data. In this study, we examine the proportional-odds cumulative logit model (Agresti, 2010) for ordered categorical data. Let $Z(s)$ be the observations at location $s \in \mathcal{D}$ with J ordered categories. Note that each ordered category corresponds to a probability $\pi(s) = \{\pi_1(s), \pi_2(s), \dots, \pi_J(s)\}$, where $\pi_i(s) = \Pr(Z(s) = i)$ for $i = 1, \dots, J$. Here, we consider $J - 1$ cumulative probabilities denoted as $\gamma_j(s) = P(Z(s) \leq j) = \pi_1(s) + \dots + \pi_j(s)$. The cumulative logit is defined as:

$$\log \left(\frac{P(Z(s) \leq j)}{1 - P(Z(s) \leq j)} \right) = \log \left(\frac{\gamma_j(s)}{1 - \gamma_j(s)} \right) = \theta_j - X(s)\beta - w(s) - \epsilon(s),$$

where θ_j is the intercept or ‘‘cutoff’’ for the j -th category, $X(s)$, β , $w(s)$ and $\epsilon(s)$ are the spatial random effects and micro-scale measurement errors. The model for the cumulative probabilities γ_j is:

$$\gamma_j(s) = P(Z(s) \leq j) = \frac{\exp\{\theta_j - (X(s)\beta + w(s) + \epsilon(s))\}}{1 + \exp\{\theta_j - (X(s)\beta + w(s) + \epsilon(s))\}}.$$

Consequently, the probabilities for the individual J categories are:

$$P(Z(s) = j) = \begin{cases} \gamma_1(s), & j = 1 \\ \gamma_j(s) - \gamma_{j-1}(s), & 2 \leq j \leq J - 1 \\ 1 - \gamma_{J-1}(s), & j = J \end{cases}$$

To avoid identifiability issues, we typically fix the first cutoff to be $\theta_1 = 0$ (Johnson and Albert, 2006). Note that the θ_j 's are constrained by the ordering $\theta_j > \theta_k$ for $j >$

k . Through a transformation (Higgs and Hoeting, 2010; Albert and Chib, 1997), we can generate unconstrained cutoff parameters $\alpha = (\alpha_1, \alpha_2, \dots, \alpha_{J-1})$, where $\alpha_1 = -\infty$, $\alpha_2 = \log(\theta_2)$, and $\alpha_j = \log(\theta_j - \theta_{j-1})$ for $j = 3, \dots, J - 1$. The inverse transformation is $\theta_j = \sum_{i=1}^{J-1} \exp\{\alpha_i\}$. The hierarchical spatial model framework is as follows:

$$\begin{aligned}
 \text{Data Model:} \quad & Z(s)|\gamma(s) \sim f(\gamma(s)) \\
 & \gamma_j(s)|\beta, \theta, \mathbf{W}, \epsilon(s) = \frac{\exp\{\theta_j - (X(s)\beta + w(s) + \epsilon(s))\}}{1 + \exp\{\theta_j - (X(s)\beta + w(s) + \epsilon(s))\}} \\
 & \theta_j|\alpha = \sum_{i=1}^{J-1} \exp\{\alpha_i\} \\
 \text{Process Model:} \quad & \mathbf{W}|\phi, \sigma^2 \sim N(\mathbf{0}, \sigma^2 R_\phi) \\
 & \epsilon(s)|\tau^2 \sim N(\mathbf{0}, \tau^2) \\
 \text{Parameter Model:} \quad & \alpha \sim p(\alpha), \quad \beta \sim p(\beta), \quad \phi \sim p(\phi), \quad \sigma^2 \sim p(\sigma^2), \quad \tau^2 \sim p(\tau^2)
 \end{aligned}$$

Precision Matrix	β_1 (95% CI)	β_2 (95% CI)	CVMPSE	Time (min)
Ind	1.07 (0.8,1.34)	0.92 (0.65,1.18)	0.28	9.53
ICAR	1.09 (0.82,1.37)	0.93 (0.67,1.2)	0.27	10.73
CAR	1.05 (0.79,1.33)	0.91 (0.65,1.18)	0.27	10.38
Gold Standard	1.03 (0.77,1.3)	0.89 (0.63,1.16)	0.29	3624.43

Table 1: Simulated example with binary spatial observations. Parameter estimation, prediction, and model fitting time results across precision matrices.

	β_1	β_2
Independent	0.88	0.93
ICAR	0.89	0.91
CAR	0.88	0.95

Table 2: Binary data simulation study: Coverage probabilities for 100 simulated samples. Columns correspond to the regression coefficients. Rows correspond to the type of precision matrix.

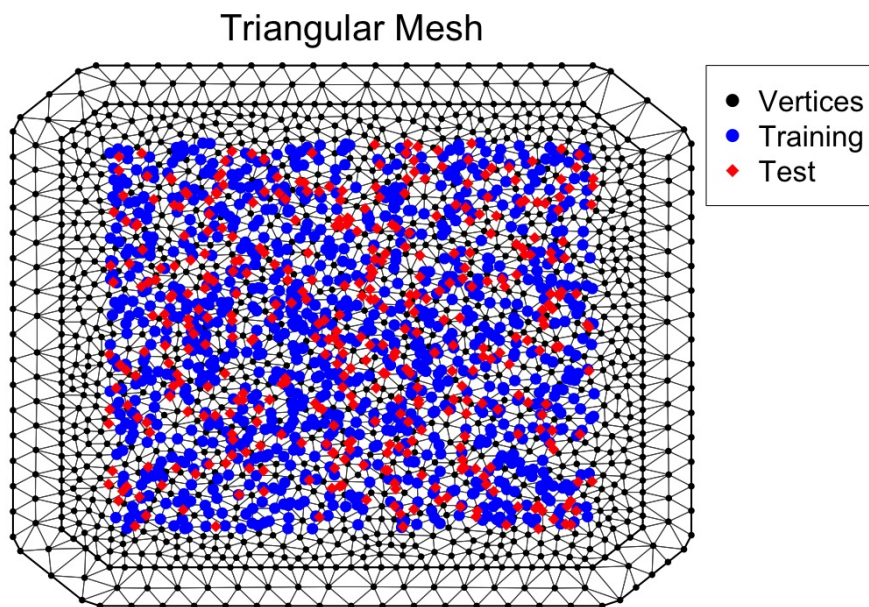


Figure 1: Triangular Mesh for data in simulation studies. Black points denote the vertices, or nodes, of the triangular mesh. Blue points represent the observation locations used to fit the hierarchical spatial models, and the red points denote the observations locations for the validation sample.

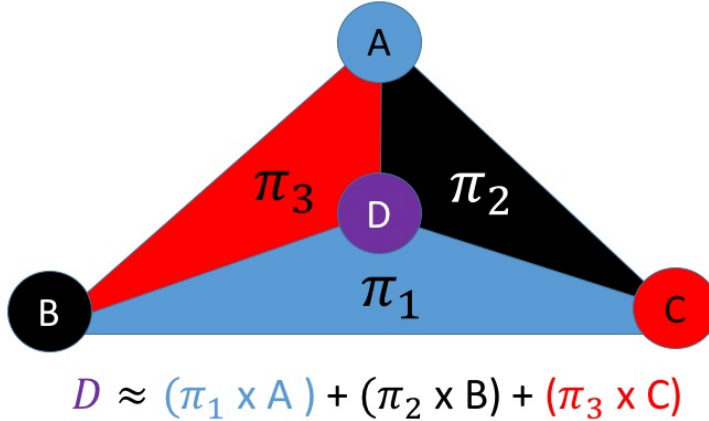


Figure 2: Diagram of the piece-wise linear basis functions. Point D is the observation location, points A , B , and C are the triangle vertices, and π_1, π_2 , and π_3 are the corresponding weights. The weights π_1, π_2 , and π_3 correspond to the proportion of the area of the specified triangle to the area of the larger triangle. We interpolate point D by taking the weighted mean of the three triangle vertices where $D \approx \pi_1 A + \pi_2 B + \pi_3 C$

2 Simulation study with spatial count observations

We conduct a simulation study using spatial count observations using 100 samples. The regression coefficients and the latent spatial random field are generated in the same way as the binary case. The observations come from a spatial generalized linear mixed model (SGLMM) with a Poisson data model and a log link function. Mesh construction and model fitting details follow closely to the binary case. We select one sample (from the 100 generated samples) as the dataset for the comparative analysis. When comparing across ranks, we elect to use the precision matrix from the ICAR model $\mathbf{Q} = (\text{diag}(\mathbf{W}\mathbf{1}) - \mathbf{W})$. We also compare inferential and predictive performance across the three different precision matrices as in the binary case.

Results indicate that the choice of rank (for the Moran’s operator) is a key driver for accurate parameter estimation and prediction as noted in Table 3. As in the binary case, the choice of precision matrices does not influence inference or prediction as shown in Table 4. Coverage probabilities (Table 5) align with the nominal coverage (95%). The PICAR approach improves mixing in the MCMC algorithm as shown by the larger effective samples per second (ESS/sec) compared to the gold standard approach. For

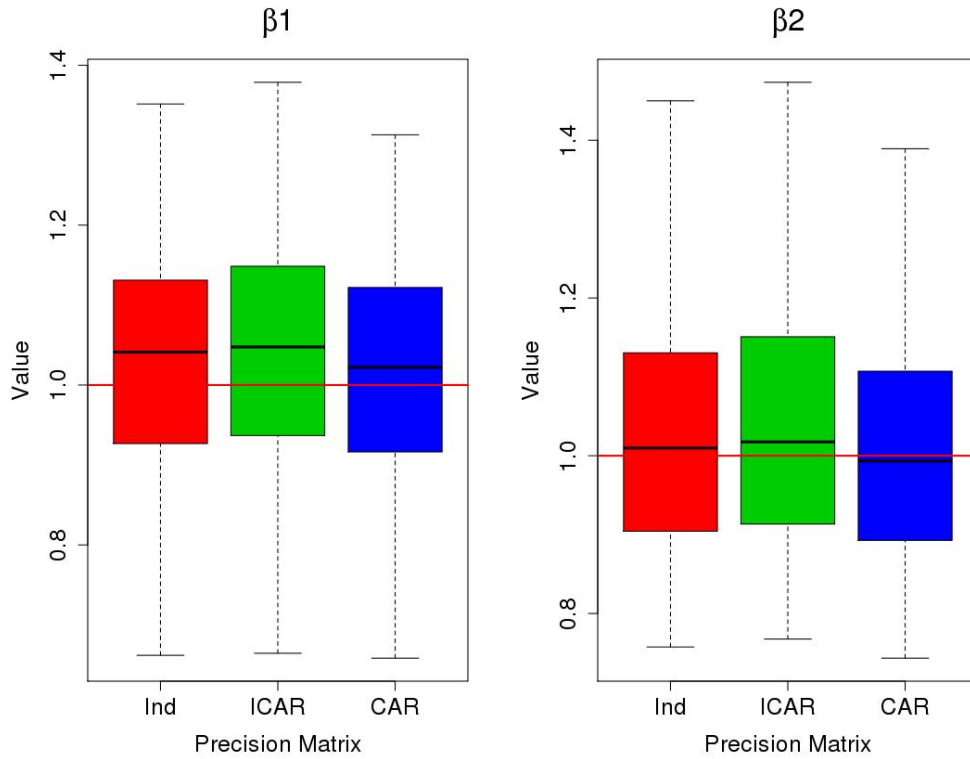


Figure 3: Binary data simulation study: distribution of posterior mean estimates for parameters β_1 (left) and β_2 (right) for three different precision matrices - Independent (red), ICAR (green), and CAR with $\phi = 0.5$ (blue). The suitable rank p of the Moran's operator \mathbf{M} chosen using the automated heuristic. Distributions are similar across precision matrices.

model parameters β_1 and β_2 , PICAR yields an ESS/sec of 6.4 and 7.2 respectively and the gold standard returns an ESS/sec 0.09 and 0.09 respectively. For the random effects \mathbf{W} , the average ESS/sec is 1.8 for the PICAR approach and 0.018 for the gold standard, an improvement by a factor of roughly 101.

Rank	β_1 (95% CI)	β_2 (95% CI)	CVMPSE	Time (min)
10	1.09 (0.99,1.19)	1.01 (0.92,1.11)	1.96	8.84
50	1.05 (0.95,1.15)	1.02 (0.92,1.12)	1.74	9.87
62	1.04 (0.94,1.14)	0.99 (0.89,1.09)	1.57	10.65
75	1.03 (0.93,1.14)	0.99 (0.89,1.09)	1.66	10.39
100	1.05 (0.95,1.16)	0.98 (0.88,1.09)	1.71	11.07
200	1.08 (0.97,1.19)	0.98 (0.87,1.1)	1.81	13.49
Gold Standard	1.07 (0.97,1.17)	1.01 (0.91,1.12)	1.66	3803.84

Table 3: Simulated example with count spatial observations. Parameter estimation, prediction, and model fitting time results across Moran’s basis ranks. Bold font denotes the rank chosen by the automated heuristic.

Precision Matrix	β_1 (95% CI)	β_2 (95% CI)	CVMPSE	Time (min)
Ind	1.04 (0.94,1.14)	0.99 (0.89,1.09)	1.56	10.92
ICAR	1.04 (0.94,1.14)	0.99 (0.89,1.09)	1.57	10.65
CAR	1.04 (0.94,1.15)	0.99 (0.89,1.09)	1.57	10.17
Gold Standard	1.07 (0.97,1.17)	1.01 (0.91,1.12)	1.66	3803.84

Table 4: Simulated example with count spatial observations. Parameter estimation, prediction, and model fitting time results across precision matrices.

	β_1	β_2
Independent	0.95	0.97
ICAR	0.95	0.96
CAR	0.95	0.95

Table 5: Poisson data simulation study: Coverage probabilities for 100 simulated samples. Columns correspond to the regression coefficients. Rows correspond to the type of precision matrix.

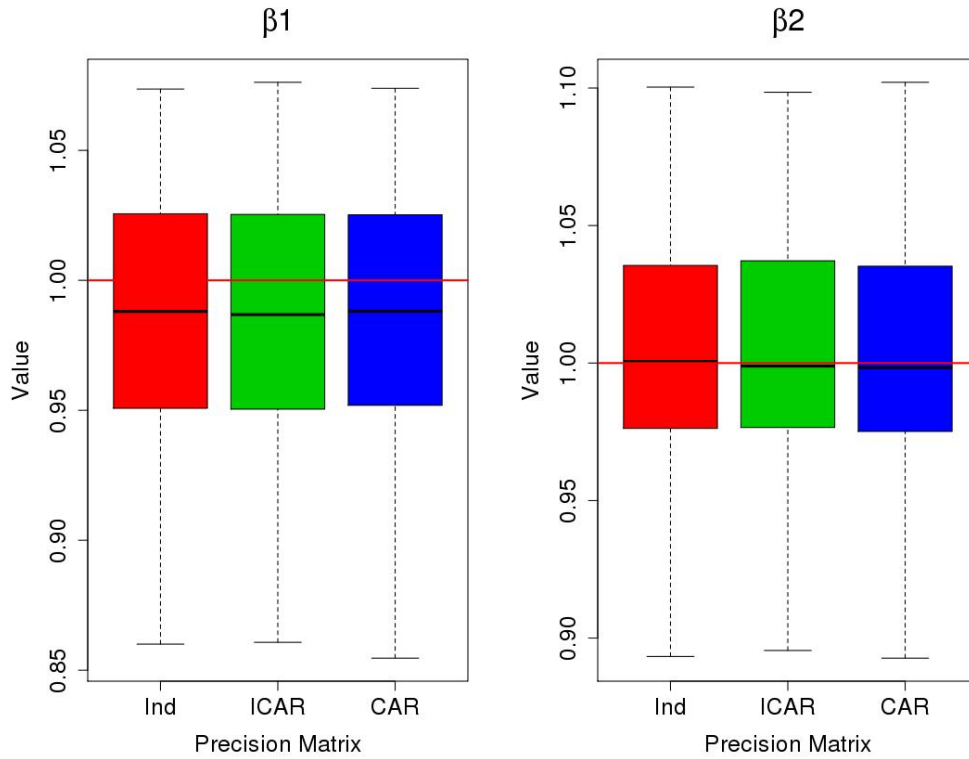


Figure 4: Poisson data simulation study: distribution of posterior mean estimates for parameters β_1 (left) and β_2 (right) for three different precision matrices - Independent (red), ICAR (green), and CAR with $\phi = 0.5$ (blue). The suitable rank p of the Moran's operator \mathbf{M} chosen using the automated heuristic. Distributions are similar across precision matrices.

	1	2	3	4	5	6
Rank	β_1 (95% CI)	β_2 (95% CI)	α_1 (95% CI)	α_2 (95% CI)	Mismatch %	Time (min)
10	0.88 (0.64,1.11)	1.01 (0.77,1.24)	-0.03 (-0.17,0.11)	-0.02 (-0.2,0.15)	0.43	12.77
23	0.9 (0.67,1.15)	1.05 (0.81,1.28)	0 (-0.14,0.14)	0 (-0.17,0.17)	0.42	12.64
50	0.94 (0.69,1.18)	1.12 (0.87,1.36)	0.05 (-0.09,0.18)	0.05 (-0.13,0.22)	0.41	13.64
75	0.98 (0.73,1.23)	1.17 (0.92,1.43)	0.07 (-0.07,0.21)	0.07 (-0.1,0.25)	0.41	14.63
100	1.01 (0.77,1.27)	1.22 (0.96,1.48)	0.09 (-0.05,0.22)	0.09 (-0.09,0.26)	0.4	16.7
200	1.12 (0.85,1.4)	1.24 (0.97,1.52)	0.15 (0.01,0.29)	0.13 (-0.05,0.3)	0.41	18.92
300	1.23 (0.94,1.52)	1.35 (1.06,1.64)	0.22 (0.08,0.35)	0.19 (0.02,0.36)	0.41	20.94
Gold Standard	0.9 (0.65,1.12)	1.07 (0.82,1.31)	0.02 (-0.12,0.16)	0.02 (-0.17,0.18)	0.42	7558.88

Table 6: Simulated example with ordered categorical spatial observations. Parameter estimation, prediction, and model fitting time results across Moran’s basis ranks. Bold font denotes the rank chosen by the automated heuristic.

	1	2	3	4	5	6
Rank	β_1 (95% CI)	β_2 (95% CI)	α_1 (95% CI)	α_2 (95% CI)	Mismatch %	Time (min)
Ind	0.9 (0.66,1.14)	1.04 (0.8,1.28)	0.01 (-0.13,0.14)	0 (-0.17,0.17)	0.42	11.70
ICAR	0.9 (0.67,1.15)	1.05 (0.81,1.28)	0 (-0.14,0.14)	0 (-0.17,0.17)	0.42	12.63
CAR	0.89 (0.65,1.12)	1.03 (0.79,1.26)	0.01 (-0.13,0.15)	0 (-0.17,0.18)	0.43	12.87
Gold Standard	0.9 (0.65,1.12)	1.07 (0.82,1.31)	0.02 (-0.12,0.16)	0.02 (-0.17,0.18)	0.42	7558.88

Table 7: Simulated example with ordered categorical spatial observations. Parameter estimation, prediction, and model fitting time results across precision matrices.

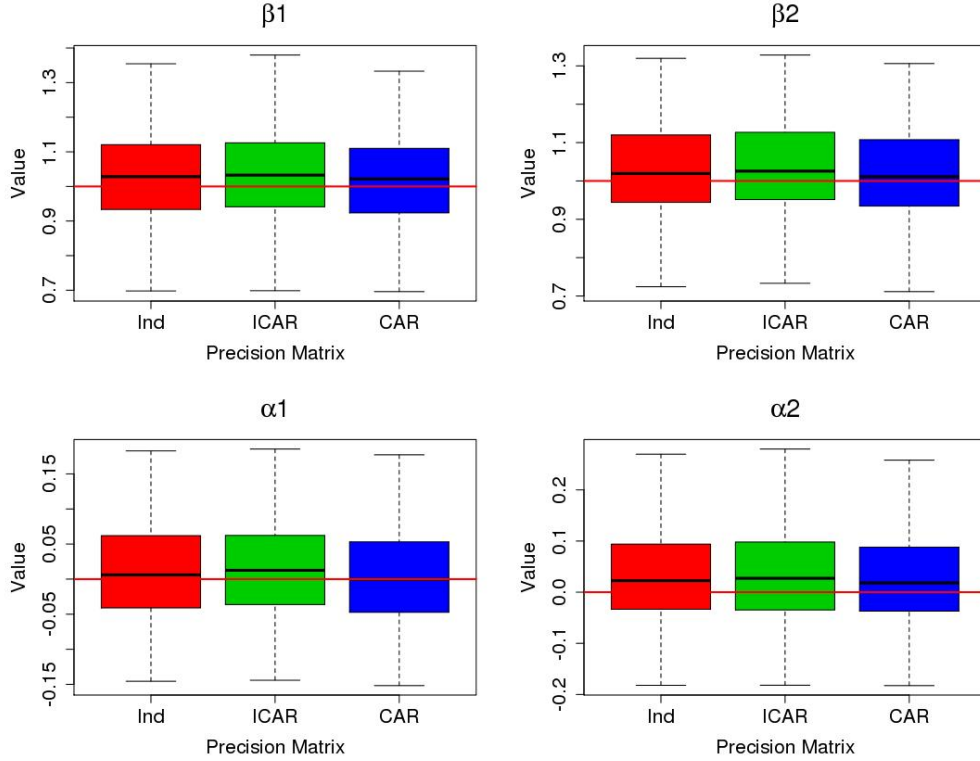


Figure 5: Ordinal data simulation study: distribution of posterior mean estimates for parameters β_1 (top left) β_2 (top right), α_1 (bottom left), and α_2 (bottom right) for three different precision matrices - Independent (red), ICAR (green), and CAR with $\phi = 0.5$ (blue). The red horizontal line denotes the true parameter values. The automated heuristic selects the appropriate rank p of the Moran’s operator \mathbf{M} . Note that the default precision matrix for the PICAR approach is the ICAR precision matrix (green). Distributions are similar across precision matrices.

3 Sparse Matrix Computations

We use the sparse matrix R package **Matrix** (Bates and Maechler, 2019) to reduce costs for the operation $\Sigma = (\mathbf{I} - \mathbf{1}\mathbf{1}'/m)\mathbf{W}$. Then, we partition the resulting matrix Σ into K mutually exclusive $\frac{1}{K} \times n$ sub-matrices Σ_k for $k = 1, \dots, K$. By parallelizing across K processors, we can quickly construct the partial Moran’s Operator $MO_k = \Sigma_k(\mathbf{I} - \mathbf{1}\mathbf{1}'/m)$ for $k = 1, \dots, K$. Finally, we generate the full Moran’s Operator by combining the MO_k ’s

	β_1	β_2	α_1	α_2
Independent	0.92	0.94	0.93	0.90
ICAR	0.91	0.92	0.93	0.88
CAR	0.93	0.96	0.93	0.94

Table 8: Ordered categorical data simulation study: Coverage probabilities for 100 simulated samples. Columns correspond to the regression coefficients. Rows correspond to the type of precision matrix.

Rank	β_1 (95% CI)	β_2 (95% CI)	CVMPSE	Time (min)
10	0.92 (0.81,1.02)	0.94 (0.85,1.03)	3.59	0.52
50	0.77 (0.54,1.01)	0.99 (0.89,1.09)	2.30	7.68
63	0.77 (0.48,1.06)	1.02 (0.9,1.12)	2.31	13.15
75	0.86 (0.55,1.16)	1.03 (0.93,1.14)	2.68	22.07
100	0.95 (0.55,1.33)	1.06 (0.94,1.17)	2.82	46.55
200	1.07 (0.7,1.49)	1.07 (0.95,1.19)	3.80	226.49

Table 9: Simulated example with spatially varying coefficients. Model fit using `stan` programming language. Parameter estimation, prediction, and model fitting time results across Moran’s basis ranks. Bold font denotes the rank chosen by the automated heuristic.

$$\text{as so } MO = \begin{bmatrix} MO_1 \\ \vdots \\ MO_K \end{bmatrix}.$$

References

- Agresti, A. (2010). *Analysis of ordinal categorical data*, volume 656. John Wiley & Sons.
- Albert, J. H. and Chib, S. (1997). Bayesian methods for cumulative, sequential, and two-step ordinal data regression models. Technical report, Bowling Green State University.
- Bates, D. and Maechler, M. (2019). *Matrix: Sparse and Dense Matrix Classes and Methods*. R package version 1.2-17.
- Gelfand, A. E., Kim, H.-J., Sirmans, C., and Banerjee, S. (2003). Spatial modeling with spatially varying coefficient processes. *Journal of the American Statistical Association*, 98(462):387–396.
- Higgs, M. D. and Hoeting, J. A. (2010). A clipped latent variable model for spatially corre-

Covariate	Estimate	95% CI
Age	0.0008	(-0.0041,0.0034)
Basal Area	-0.0045	(-0.007,-0.0026)
Height	0.0203	(0.0157,0.0236)
Volume	-0.0026	(-0.0034,-0.0017)
tau	0.0040	(0.0021,0.0094)

Table 10: Inference results for the mistletoe data. Rows correspond to the predictor variables and columns include the parameter estimates and 95% credible intervals

lated ordered categorical data. *Computational Statistics & Data Analysis*, 54(8):1999–2011.

Johnson, V. E. and Albert, J. H. (2006). *Ordinal data modeling*. Springer Science & Business Media.

Schliep, E. M. and Hoeting, J. A. (2013). Multilevel latent Gaussian process model for mixed discrete and continuous multivariate response data. *Journal of agricultural, biological, and environmental statistics*, 18(4):492–513.

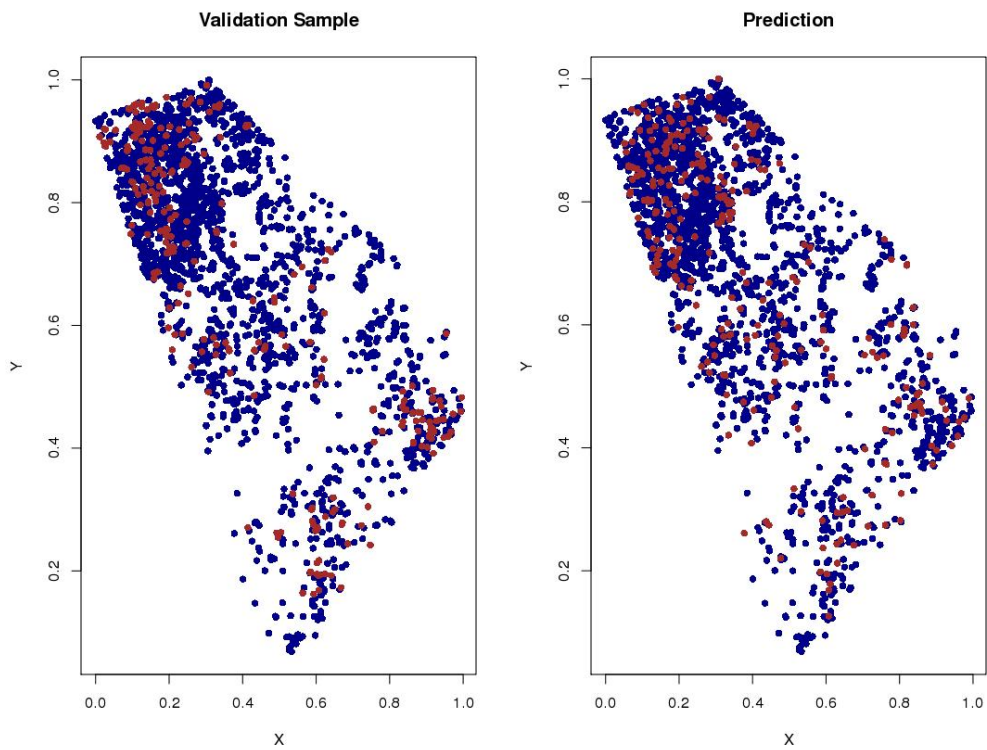


Figure 6: Observed (left) and predicted (right) dwarf mistletoe presence and absence at the validation sample locations. Red points denote the presence of dwarf mistletoe and blue points denote absence.

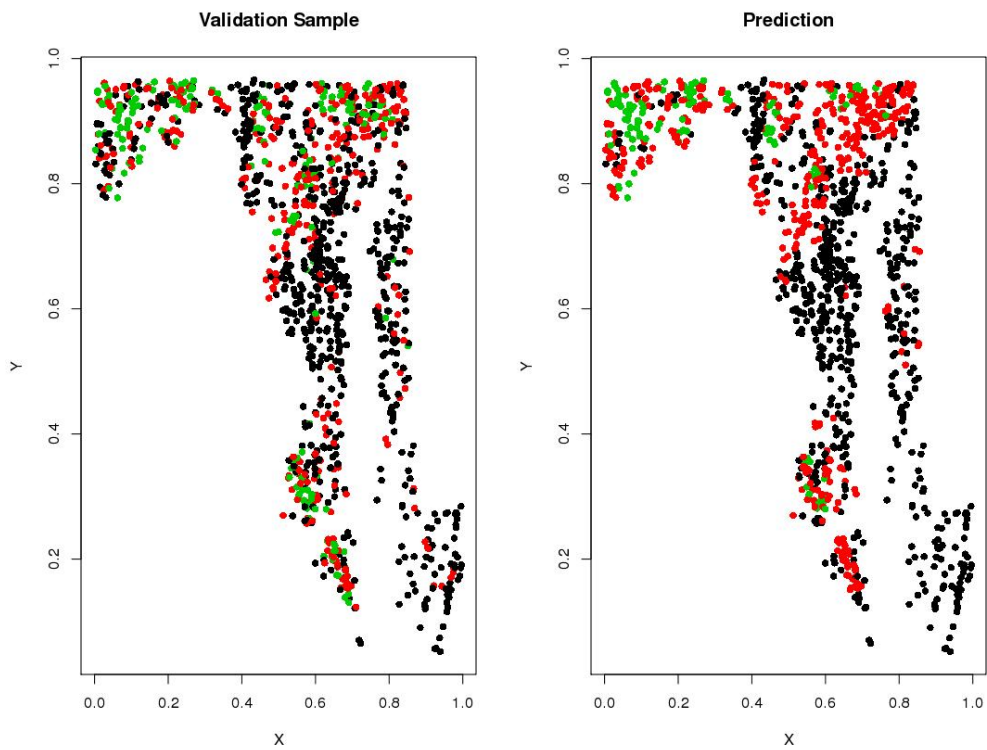


Figure 7: The left panel shows the BIBI index at the prediction locations and the right panel shows the predicted BIBI index. Black, red, and green points indicate low, medium and high levels of BIBI respectively.

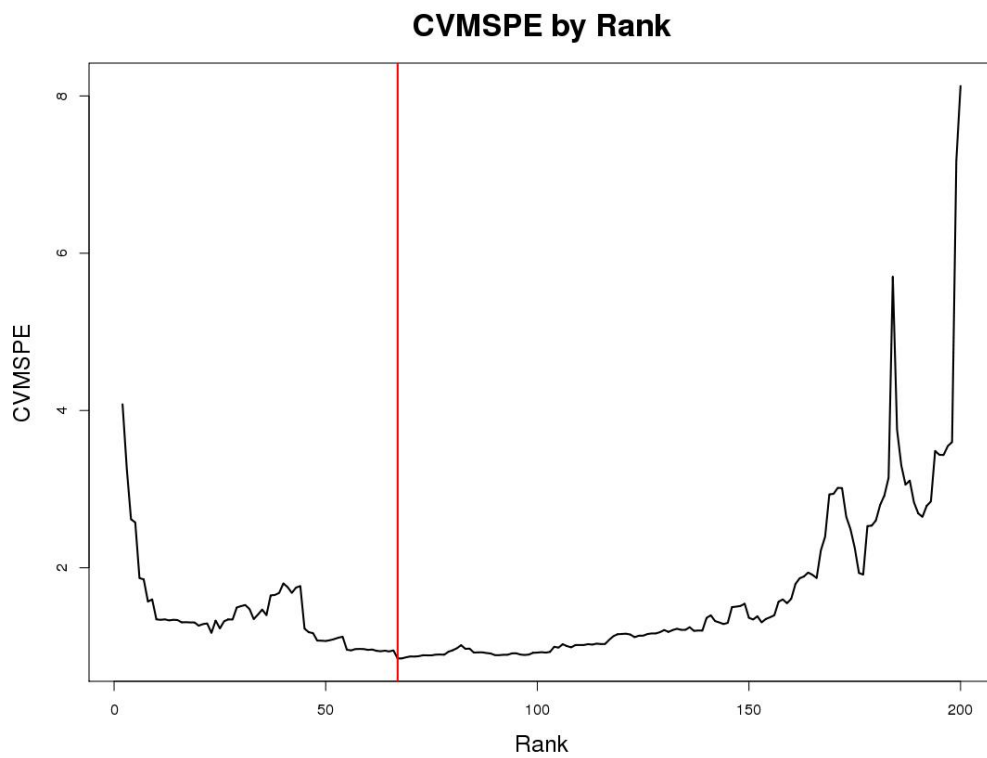


Figure 8: Cross-validated mean squared prediction error (CVMSPE) for ranks 1-200 using the automated heuristic. The vertical red line denotes the chosen rank ($p = 63$) with lowest CVMSPE.